Segmented Differential Power Processing Converter Unit and Control Algorithm for Photovoltaic Systems

Hoejeong Jeong, *Student Member, IEEE*, Seungbin Park, Jee-Hoon Jung, *Senior Member, IEEE*, Taewon Kim, A-Rong Kim, and Katherine A. Kim, *Senior Member, IEEE*

***Abstract*—Differential power processing (DPP) for photovoltaic (PV) systems can achieve high system efficiency and maintain maximum power production even under mismatched conditions. However, DPP converters applied to large-scale systems have challenges of complicated installation and high voltage ratings. The segmented DPP structure is introduced as a modular approach that utilizes groups of bidirectional DPP flyback converters to maximize PV power generation while minimizing converter power loss. Groups of four DPP converters are combined into a segmented DPP unit with maximum power point tracking (MPPT) control to maximize output power of the unit. The segmented DPP system and control algorithm are verified through simulation and hardware experimentation. Simulation results verify the effectiveness of the control algorithm with multiple segmented DPP units interacting with a typical inverter employing MPPT. Experimental results verify that system efficiency of the segmented DPP unit reaches 96.4% in even lighting conditions, reaches 92.7% in severe partial shading conditions, and shows an increase of up to 14.8% in uneven lighting conditions compared to an equivalent series-connected PV system.**

***Index Terms*—Bidirectional flyback converter, dc–dc converter, differential power processing (DPP), maximum power point tracking (MPPT), partial power processing, photovoltaic (PV) systems.**

I. Introduction

In SOLAR photovoltaic (PV) systems that provide renewable energy to the electric grid, PV panels are typically connected in series to achieve high voltage required for grid connection. A power converter controls the PV panels to operate at the maximum power point (MPP) of the series string and transfers power to the load. However, series-connected PV panels cannot always generate maximum power because mismatch among the panels, due to shading or uneven sunlight, can severely reduce the power output. To overcome this problem, full power processing (FPP) systems like dc optimizers or modular integrated converters (MIC) are widely used [1]. These FPP converters are normally connected to each PV panel to convert and control power from each PV panel individually [2], [3]. With individual control, the PV panels can generate near-maximum power, but the converters process the full power of the PV panels, which contributes to losses that are proportional to the power level. Thus, the PV-to-output system efficiency in an FPP system cannot exceed the power converter efficiency.

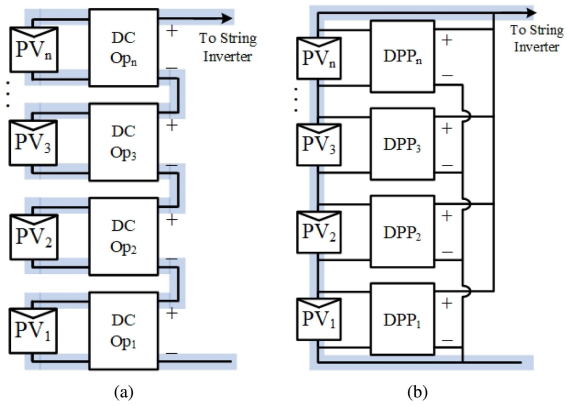

Fig. 1. Main current flow of (a) FPP and (b) DPP systems.

Differential power processing (DPP) systems have been studied to achieve high efficiency under partial shading and mismatched conditions [4]. DPP converters are also connected to each PV panel, like FPP converters, but the architecture is fundamentally different. When the PV panels experience mismatch, the DPP converters transfer a small amount of power to maintain MPP operation [5], [6]. In other words, DPP systems process a smaller amount of power compared to FPP systems. Fig. 1 shows the main current flow of FPP and DPP systems. As shown, in the FPP system, the main power flows through the FPP converters, which process the full amount of PV power. Conversely, in the DPP system, the main power flows through the PV panels and the DPP converters process a small amount of power, rather than full PV power. For this reason, the power rating of the DPP converter

Manuscript received April 20, 2020; revised July 7, 2020, August 27, 2020, and November 9, 2020; accepted December 8, 2020. Date of publication December 14, 2020; date of current version March 5, 2021. This work was supported in part by the Research Institute of Industrial Science and Technology (RIST), Korea, through the grant on DPP Technique Development for Improving PV Efficiency under Grant 2017A032 and in part by the Ministry of Science and Technology, Taiwan, under Grant 109-2218-E-002-011-MY3. Recommended for publication by Associate Editor S. Mekhilef. *(Corresponding author: Katherine A. Kim.)*

Hoejeong Jeong, Seungbin Park, and Jee-Hoon Jung are with the School of Electrical and Computer Engineering, Ulsan National Institute of Science and Technology (UNIST), Ulsan 44919, South Korea (e-mail: hjeong94@unist.ac.kr; spsb95@unist.ac.kr; jhjung@unist.ac.kr).

Taewon Kim and A-Rong Kim are with the Research Institute of Industrial Science and Technology, Pohang 37673, South Korea (e-mail: robokim@rist.re.kr; arkim83@rist.re.kr).

Katherine A. Kim is with the Department of Electrical Engineering, National Taiwan University, Taipei 10617, Taiwan (e-mail: kakim@ntu.edu.tw).

Color versions of one or more figures in this article are available at https://doi.org/10.1109/TPEL.2020.3044417.

Digital Object Identifier 10.1109/TPEL.2020.3044417

Fig. 2. Different colored BIPV installed on a building[8].

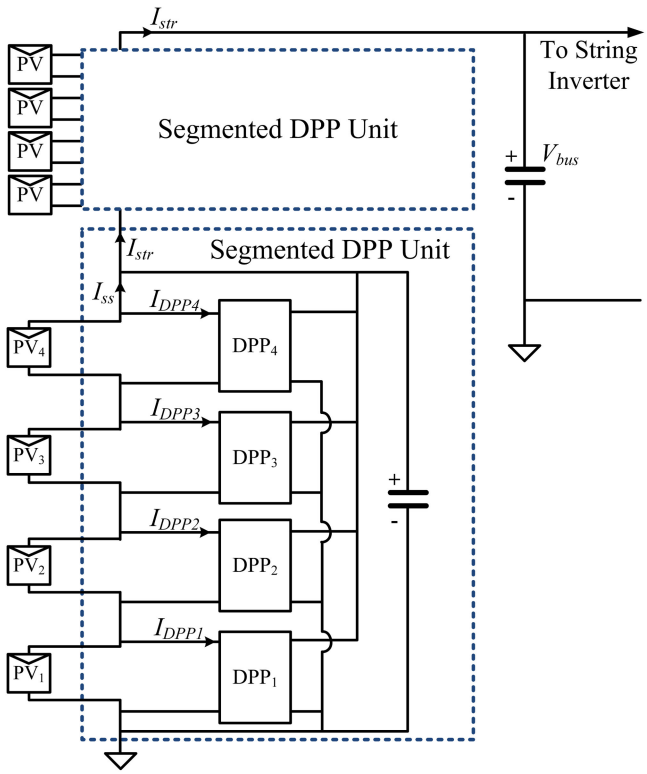

Fig. 3. Segmented DPP unit connection diagram.

is lower than that of the FPP converter such that converter loss and component cost can be lower. Also, since full power is not always flowing through the DPP converters, the wear of the DPP converters can be reduced, which has reliability benefits.

DPP converters are particularly conducive to PV installations that are frequently exposed to uneven lighting conditions. Building-integrated photovoltaic (BIPV) systems are one such example, where PV panels are often installed at different angles because they are integrated into the building structure [7]. In this article, the target application is a BIPV system where PV panels are installed vertically on the wall of a building. Each PV panel is covered with a sheet of glass, but the sheets of glass are tinted with different colors for purely aesthetic reasons to match the building's design, as shown in Fig. 2 [8]. In this installation, the PV panels experience both slight mismatch, in both illumination and temperature, due to the glass tinted with different colors and severe mismatch due to building self-shading at certain times of the day. With the level of mismatch expected in this type of BIPV installation, DPP converters are chosen for their ability to yield higher efficiency and performance compared to series-connection or FPP converters.

An example of the DPP architecture referred to as PV-to-bus [9] is shown in Fig. 1(b). In this architecture, each DPP converter is connected between a PV panel and the PV string voltage, where the PV string voltage is equivalent to the system bus voltage. Previous work has validated various converter topologies for PV-to-bus DPP converters, including the flyback [10], multistacked LLC resonant [11], and multistacked SEPIC [12]. Ideally, each PV-to-bus DPP converter is bidirectional such that it supplies or draws current to maintain MPP operation of the PV panel [9]. When the PV-to-bus system operates at the unique minimum where the least amount of power is processed, the system achieves higher output power than FPP converters and, generally, better performance than other DPP architectures such as PV-to-PV converters, which connect between a PV panel and an adjacent PV panel [13].

DPP converters have shown clear advantages in higher power production and lower converter ratings, yet they have still not gained traction in the commercial market [4]. One major challenge is in the implementation of previously proposed DPP architectures, particularly, for high-voltage grid-connected PV systems. For DPP systems to be commercially viable, increased energy capture must be achieved at lower or equivalent cost of existing PV converter systems. Further, system installation should be straightforward to reduce labor costs and minimize the chance of incorrect installation. The converter system should also be modular such that it could be scaled up without the need for completely redesigning or rewiring the entire system. Thus, for PV DPP systems to be widely adopted, they should have a cost-effective modular design that improves overall system efficiency.

To meet these needs, this article proposes a *segmented DPP* system, as shown in Fig. 3, which is modular and requires minimal connections. In this architecture, groups of DPP flyback converters are modularized into a unit that is controlled and operates independently. This structure enables the DPP converters to be designed with lower voltage stresses and low cost.

The work in [14] proposed a DPP architecture that connected between the PV panels and an isolated bus, which also benefited from lower voltage ratings on the isolated bus side. It was implemented at the submodule level of a PV panel, which is also a type of segmented DPP system if the submodule DPP units are connected in series. However, [14] does not explore or analyze the effect of connecting the submodule DPP units in series. Also, [14] uses voltage balancing control of the three substrings of a PV panel, which works well when the PV MPP voltages are nearly equal. However, it is less effective in systems that experience severe mismatch, particularly when temperature varies between PV panels, causing the PV MPP voltages to vary

[15], [16]. Since temperature variation is expected in the target BIPV application, individual MPPT control is a requirement.

Earlier work in [17] introduced, explored, and validated the segmented DPP concept but only referred to it as a unit DPP converter. It consisted of flyback converters that controlled PV operation by processing power between the PV and a shared bus, and a boost converter that controlled the voltage of the shared bus by processing power between the shared bus and the stacked PV string. The maximum system efficiency achieved with that work was 94.7% under even lighting conditions. This article improves on the concept by removing the boost conversion stage to simplify the structure and further increase conversion efficiency. This article also details the control algorithm that allows for individual MPPT of the PV panels connected to the segmented DPP unit.

The contributions of this article are the introduction of the segmented DPP topology, development of an individual MPPT control algorithm with minimal sensor requirements that independently controls each segmented DPP module, experimental validation of the modular segmented DPP unit, and experimental results of the system's improved performance over existing solutions. The final results show effective operation of a segmented DPP module consisting of four bidirectional flyback converters, and high system efficiency, up to 96.4% under even lighting conditions.

II. Modularity and Cabling

Modularity and ease of installation are critical for wider commercial acceptance of PV DPP systems. Also, additional cables and connectors needed for DPP converters add manufacturing cost such that additional wiring should be minimized. Standard PV panels are manufactured with a watertight junction box that has two standard-length cables and standard watertight MC4 connectors. DPP systems should easily interface with these standard PV panel cables and be straightforward to install.

A. PV-to-Bus DPP

In designing PV-to-bus DPP converters, one challenge is the high voltage step-up ratio from the PV-side to the bus-side. In a string of n PV panels, the output voltage of the DPP converters should be rated to boost n times the input voltage. While this is reasonable for small values of n, it is problematic for long strings of PV panels. Also, the physical wire connections of a PV-to-bus DPP system are complicated and require numerous connections. If the PV-to-bus architecture is implemented with n individual DPP converters, each DPP converter requires eight connectors: two for the PV, three for one adjacent DPP converter, and three for the other adjacent DPP converter. For a system of n PV panels, the total number of connectors is $8n$ and the number of additional cables (excluding PV panel cables) is $3(n-1)+4$.

B. Segmented DPP

Segmented DPP addresses these challenges by being modular, using a minimal number of connections, and reducing the number of additional cables to allow for straightforward installation. In this approach, the original PV-to-bus architecture is segmented such that the output voltage of the DPP converters is not the entire PV bus but the voltage of a smaller subset of PV panels. Adjacent PV panels are connected to one segmented DPP unit that consists of multiple DPP converters. Then, the DPP units are connected together to form the overall string. The standard PV cable length should connect a panel to the nearest segmented DPP unit. For n PV panels, let m be the number of PVs connected to one PV unit such that there are n/m DPP units. Then, each DPP unit has $2(m+1)$ connections: two for each PV panel connected to the unit and two for the adjacent DPP units.

As a point of comparison, dc optimizers are commonly implemented as an additional unit that attaches to the backside of each panel. The two standard PV cables connect to the dc optimizer unit and two additional cables with standard MC4 connectors connect to the adjacent dc optimizer units, one for each side. For n PV panels, each dc optimizer unit has $4n$ connections and $2n$ cables. Since dc optimizers have been commercialized for many years in the PV industry, the number of connectors and cables is considered a baseline for industry acceptance.

Fig. 4 shows the connectors and cables for a segmented DPP system viewed from behind the PV panels for $m=4$. Table I summarizes the number of connectors and cables needed for the conventional PV-to-bus implementation, dc optimizers, and the segmented DPP architectures; it also gives the numbers for

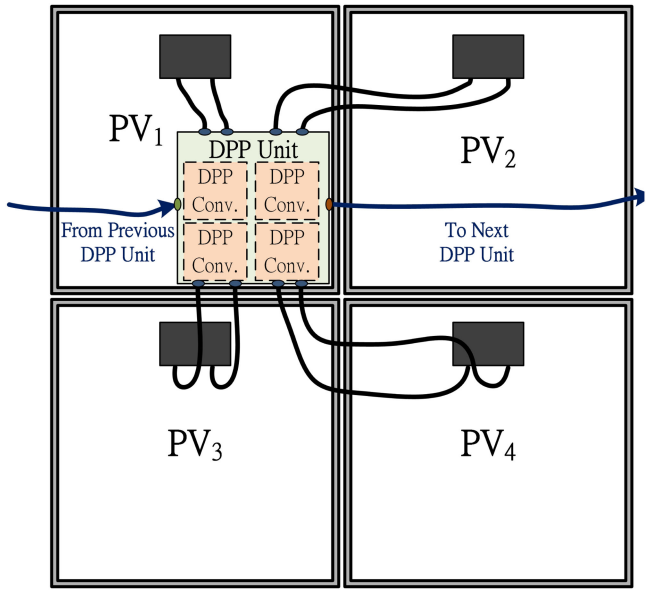

Fig. 4. Segmented DPP architecture connectors and cables.

TABLE I
Connectors and Cables for DPP Architectures

Architecture	Number of		Ex: $n=12$	
	Conn.	Cables	Conn.	Cables
PV-to-bus	$8n$	$3(n-1)+4$	96	132
dc optimizer	$4n$	$2n$	48	24
seg. DPP ($m=4$)	$\frac{5}{2}n$	$\frac{n}{4}+1$	30	4
seg. DPP ($m=6$)	$\frac{7}{3}n$	$\frac{n}{6}+1$	28	3

an example case of $n = 12$ PV panels. The PV-to-bus system requires 96 connectors and 132 cables for 12 PV panels, which is significantly more than the dc optimizer system that requires 48 connectors and 24 cables. Conversely, the segmented DPP systems require 30 connectors or fewer and only 3–4 cables. The segmented DPP approach has a significantly lower connector cost and fewer cables to ease installation such that segmented DPP is viable for commercialization and industry acceptance.

III. Segmented DPP System

The segmented DPP system is proposed to reduce wiring complexity, lower the high step-up ratio of the converter, and improve modularity, compared to the existing PV-to-bus DPP system. Although the architecture is based on the PV-to-bus architecture, its structure and operation are fundamentally different. It has unique challenges in terms of converter design and control.

A. Structure of the Segmented DPP System

In the segmented DPP architecture, each segmented DPP unit consists of m DPP converters connected to m PV panels. Fig. 3 shows an example of segmented DPP system connected to four PV panels where $m = 4$. The input of each DPP converter is connected to one PV panel and the output of each DPP converter is connected to the series connection of m PV panels. Each DPP converter controls its adjacent PV panel at its MPP and operates bidirectionally to transfer power from the PV panel to the string of m panels or vice versa. The DPP converters need galvanic isolation between input and output because the DPP converter inputs are connected in series while the DPP converter outputs are connected in parallel; thus, the primary and secondary ground should be isolated.

The segmented DPP unit is modular and scalable such that m PV panels are connected to a unit and, then, units can be connected in series to form the string that connects to the string inverter. One practical design requirement is that the standard PV panel cables should be able to connect to the segmented DPP module for ease of installation. Based on physical constraints of the standard-length cables, the number of PV connections is generally limited to $m < 9$ (3 by 3 panel configuration connecting to one unit). There is a basic tradeoff between the number of panels connected to one segmented DPP unit and system performance. The value of m is related to the number of panels that can exchange power with each other in order to offset mismatch. A larger value of m means that the unit will balance power among more PV panels in the string. Conversely, a lower value of m means that the unit will balance power among fewer PV panels, which can lower overall performance at the string level. However, a lower value of m decreases the segmented DPP converter's voltage boost ratio and reduces the connections to one unit. In this article, the selection of m is based on considerations of physical connections, performance, and testing capabilities for the target BIPV application. A design with four PV panels connected to one unit, $m = 4$, was selected.

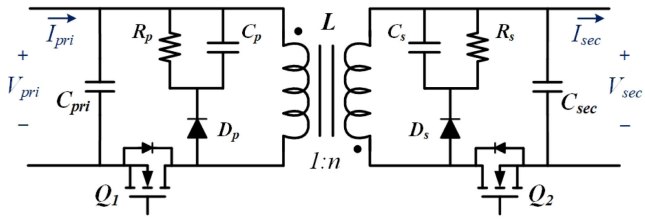

Fig. 5. Circuit of the bidirectional flyback converter.

TABLE II
Bidirectional Flyback Converter Design Parameters

Parameter	Primary	Secondary
Voltage	12.8 V	51.2 V
Current	±2.0 A	±0.5 A
Switching frequency	100 kHz	
Coupled inductor turns	7	19
Magnetizing inductance	8.9 μH	64.88 μH
Leakage inductance	0.25 μH	1.92 μH
Snubber Capacitance	200 nF	10 nF
Snubber Resistance	1.2 kΩ	23.5 kΩ

B. Bidirectional Flyback DPP Converter

This work examines a segmented DPP unit with $m = 4$, which shows the benefits of the architecture while maintaining a moderate converter output voltage. The DPP converter used is a bidirectional flyback converter [14], [18]. Bidirectional operation is needed because the converter should take extra power away when the MPP current of the PV is higher than the substring current (I_{SS}) and provide additional power to the PV when the MPP current is lower than I_{SS}. In this way, the DPP converter can maintain PV operation at the MPP current, regardless of I_{SS} [4]. Fig. 5 shows the circuit diagram for the bidirectional flyback converter, where the diode of the unidirectional flyback converter is replaced by a MOSFET. For forward operation, MOSFET Q_1 is driven and the body diode of Q_2 acts as a diode; for reverse operation, Q_2 is driven and the body diode of Q_1 acts as a diode.

1) Converter Design: The voltage rating of the DPP converter depends on the PV panel open-circuit voltage V_{oc} and the number of panels connected to one DPP unit m. The primary side is rated at V_{oc} of the PV panel and the secondary side is rated at mV_{oc}. The nominal voltage ratings of the converter are based on the panel's MPP voltage V_{mpp} at which the PV panels usually operate. For this work, $V_{oc} = 16$ V, $V_{mpp} = 12.8$ V, and $m = 4$. The converter current rating is directly related to the expected current mismatch of the PV panels. The work in [13] identified power ratings at 15%–17% of the panel rating to compensate for mild PV mismatch in PV-to-bus converter systems. For this work, the current limit was chosen as 2.0 A for PV panels with MPP current of 8.3 A, which is equivalent to 24% of the panel rating. The flyback converter design parameters are shown in Table II. RCD snubbers are used on both the primary and secondary sides, as shown in Fig. 5. The snubber reduces the high voltage over the MOSFET caused by the resonance between the leakage inductance and switch capacitance. Each snubber is designed according to [19] such that the snubber capacitance

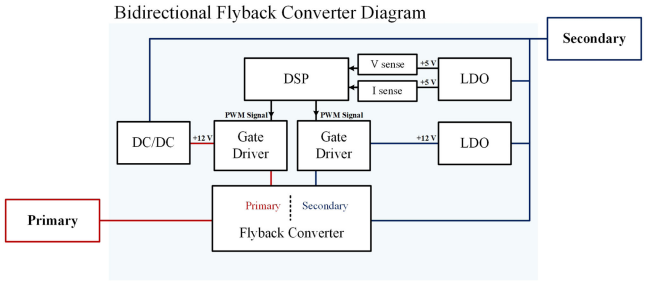

Fig. 6. System diagram of the bidirectional flyback converter.

and resistance values differ based on parameters of each side [20], as outlined in Table II.

To operate the two MOSFET switches, gate drivers on both the primary and secondary sides are needed, where both drivers require a steady 12-V supply. Because the voltage of one PV panel may be lower than 12 V in some operating conditions, power is supplied from the secondary-side voltage, which is a reliably high voltage. However, since the primary-side gate driver ground should be separated from the secondary-side ground, a low-power isolated dc–dc converter is used for the primary-side gate driver and a low dropout (LDO) linear regulator is used for the secondary-side gate driver. An additional LDO linear regulator powered from the secondary side to 5 V is used to supply power to the voltage and current sensors of the converter. Fig. 6 shows the diagram of the bidirectional flyback converter.

2) Converter Operation Mode: A flyback converter can be designed to operate in continuous conduction mode (CCM) or discontinuous conduction mode (DCM). In CCM, the body diode needs time for reverse recovery due to the characteristics of the MOSFET body diode. This causes a large peak and ripple current through the driven switch, which causes reverse recovery loss. In DCM, the input side switch is turned ON when the output side current has already reached zero such that there is no reverse recovery loss. Also, there is no right half plane zero in DCM, which makes the compensation feedback control loop easier to design. Thus, the bidirectional flyback converter was designed for DCM operation.

As a segmented DPP converter, the flyback converter should control the primary-side current I_{pri} to a positive value in forward mode and a negative value in reverse mode. Let D_1 be the duty ratio for Q_1 in forward mode and D_2 be the duty ratio for Q_2 in reverse mode. For DCM operation, the voltage gain in the forward direction [21] is

$$\frac{V_{\text{sec}}}{V_{\text{pri}}} = D_1\sqrt{\frac{V_{\text{sec}}T}{2L_{\text{mp}}I_{\text{sec}}}} \tag{1}$$

where V_{sec} is the secondary-side voltage, V_{pri} is the primary-side voltage, T is the switching period, L_{mp} is the primary-side magnetizing inductance of the coupled inductor, and I_{sec} is secondary-side current. Solving for D_1 and using power balance to substitute in I_{pri} yields

$$D_1 = \sqrt{\frac{2L_{\text{mp}}I_{\text{pri}}}{V_{\text{pri}}T}}. \tag{2}$$

Similarly, the voltage gain in the reverse direction is

$$\frac{V_{\text{pri}}}{V_{\text{sec}}} = D_2\sqrt{\frac{V_{\text{pri}}T}{2L_{\text{ms}}(-I_{\text{pri}})}} \tag{3}$$

where L_{ms} is the secondary-side magnetizing inductance of the coupled inductor and $-I_{\text{pri}}$ is the current flowing out of the primary side. Then, solving for D_2 yields

$$D_2 = \sqrt{\frac{2L_{\text{ms}}V_{\text{pri}}(-I_{\text{pri}})}{V_{\text{sec}}^2T}}. \tag{4}$$

Equations (2) and (4) show that both duties D_1 and D_2 can be expressed in terms of I_{pri} such that they can be used to control the primary-side current in both forward and reverse modes of the DPP flyback converter.

IV. Segmented DPP Control Algorithm

The goal of the segmented DPP control algorithm is to maximize PV power production while reacting quickly to light changes. Two control modes are proposed for the segmented DPP unit: voltage balancing to quickly bring the operating point near the MPP and MPPT to reach the true MPP for each panel. Both control modes operate by setting the primary-side current value of each bidirectional DPP flyback converter. A PI controller is used to regulate the primary-side current to the reference value for each converter. When the reference current is positive, the DPP converter operates in the forward direction. When the reference current is negative, the DPP converter operates in the reverse direction. When the reference current is zero, the converter turns off to reduce unnecessary switching losses.

A. Voltage Balancing Mode

Even when a set of PV panels experience different illumination levels, their MPP voltages are similar [22]. For this reason, balancing or equalizing the PV panel voltages brings their voltages near the MPP [23] but not necessarily to the exact value. Fig. 7 shows the flowchart of the proposed voltage balancing algorithm for segmented DPP units.

Based on the characteristics of PV panels, the voltage of a panel decreases when current increases. Hence, if the measured voltages of all the PV panels are not in a certain range, the index of the panel with the highest voltage is identified, and the reference current of that index is increased by a set value ΔI to decrease that panel's voltage. The index of the panel with the lowest voltage is also identified and the reference current is decreased by ΔI to increase that panel's voltage. By increasing and decreasing the reference currents by the same amount, the return current I_r and substring current I_{ss} (denoted in Fig. 3) remain approximately constant such that the other PV panels of the unit are not affected. The algorithm then waits for a set amount of time, during which the segmented DPP system's operating point stabilizes. Then, the algorithm starts again by measuring the new PV voltages. Once all PV panel voltages are within the set range, the control mode switches to the MPPT mode. At any point in operation, if the PV panel voltages fall outside of the set range due to sudden illumination changes,

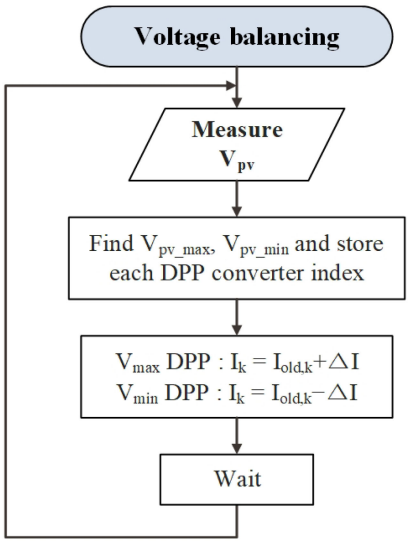

Fig. 7. Voltage balancing algorithm for segmented DPP.

the controller returns to voltage balancing mode until the PV voltages are again within the set range.

B. Maximum Power Point Tracking Mode

After the voltage balancing algorithm runs, each PV panel operates near its MPP. Then, the MPPT algorithm is used to ensure operation at the individual MPP of each PV panel. The MPPT control algorithm follows a similar approach to the perturb and observe (P&O) algorithm [24], [25] but is adapted to the unique segmented DPP system. Fig. 8 shows the flowchart of the MPPT algorithm for a segmented DPP unit. By design, the MPPT algorithm runs significantly faster than the inverter MPPT algorithm that controls the string current I_{string}. This means that I_{string} is assumed to be constant while the MPPT algorithm executes such that the total PV voltage is proportional to the power produced by the segmented DPP unit. Thus, the algorithm aims to maximize total PV voltage which is equivalent to maximizing power production.

First, each PV panel voltage is measured and the sum of m PV voltages is calculated. Then, the primary-side reference current of the first DPP converter is incremented by a set amount and the system adjusts to the new operating point. Next, the total PV voltage is calculated again and compared to the previous total voltage. If the total voltage increases, the system maintains the new reference current. However, if the total voltage decreases, the reference current returns to the previous value and the direction of the increment is changed for that converter. This procedure is executed sequentially for each converter until it reaches the last converter and then returns to the first converter again.

The operating points of the PV panels and the DPP converters are highly coupled; so the reference currents of the converters are changed one by one rather than changing all the reference currents at once. When the string current changes, the MPPT algorithm maximizes the voltage based on the new I_{string} value.

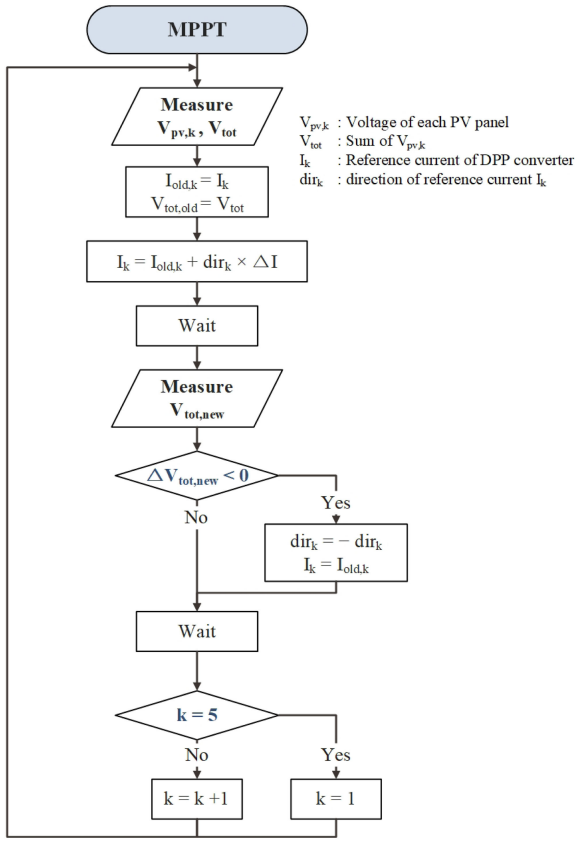

Fig. 8. MPPT algorithm for segmented DPP.

In this way, the system is continually adjusting its operating point to stay as close as possible to the MPP of the segmented DPP unit, thus maximizing the output power for the given I_{string} value.

C. Sensor Requirements

Both voltage balancing and MPPT modes rely only on PV panel voltage measurements to adjust the converter current references. Thus, each PV panel needs a voltage sensor at the primary side of the DPP converter and each DPP converter requires one current sensor on the primary side, which is a total of $2m$ sensors. The proposed control algorithm has the advantage of requiring a small number of sensors in the segmented DPP unit, which reduces power loss in the sensors, board area, converter cost, and controller computation time.

V. Segmented DPP System Simulation

To verify the segmented DPP system structure and control algorithm, a model was developed in MATLAB Simulink. Fig. 9 shows the simulation diagram of the segmented DPP unit, which consists of four PV panels and four DPP flyback converters with one controller. Fig. 10 shows the simulation diagram of the bidirectional flyback converter, including the PI controller for the bidirectional primary-side current (I_{DPP}). The primary-side voltage (V_{pv}) is measured and used as an input for the

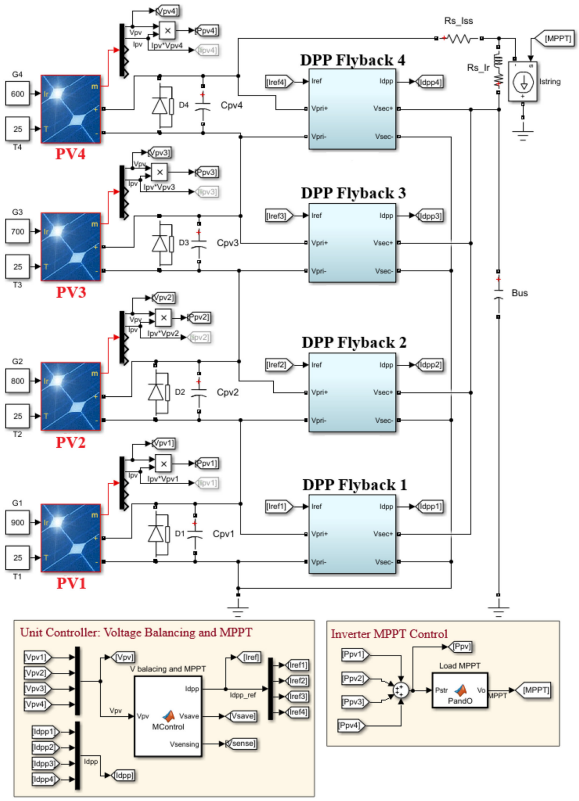

Fig. 9. Segmented DPP unit simulation diagram.

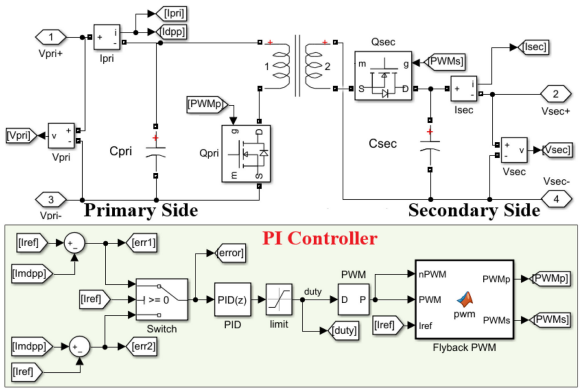

Fig. 10. Bidirectional flyback converter simulation diagram.

segmented DPP unit control algorithm. After the algorithm sets the reference current I_{ref}, the PI controller adjusts the converter to regulate I_{DPP} to I_{ref}. The segmented DPP unit is connected to a controlled current source block, which emulates the inverter to control the string current using the conventional P&O MPPT algorithm. The simulated PV panel has a nominal power of 106 W at 1000 W/m^2 and 25 °C, which is based on the PV panel designed for this BIPV application. In the simulations, irradiance levels on each of the PV panels were varied to emulate an example with different lighting levels. Fig. 11 shows the power-voltage curve and MPP of the simulated PV panel at 900, 800, 700, and 600 W/m^2.

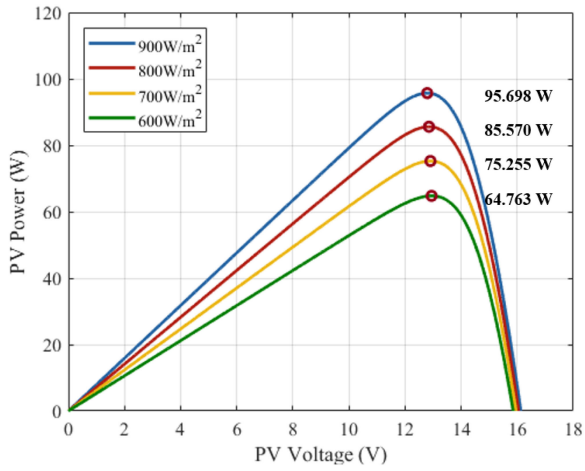

Fig. 11. Power-voltage curves for the simulated PV panel.

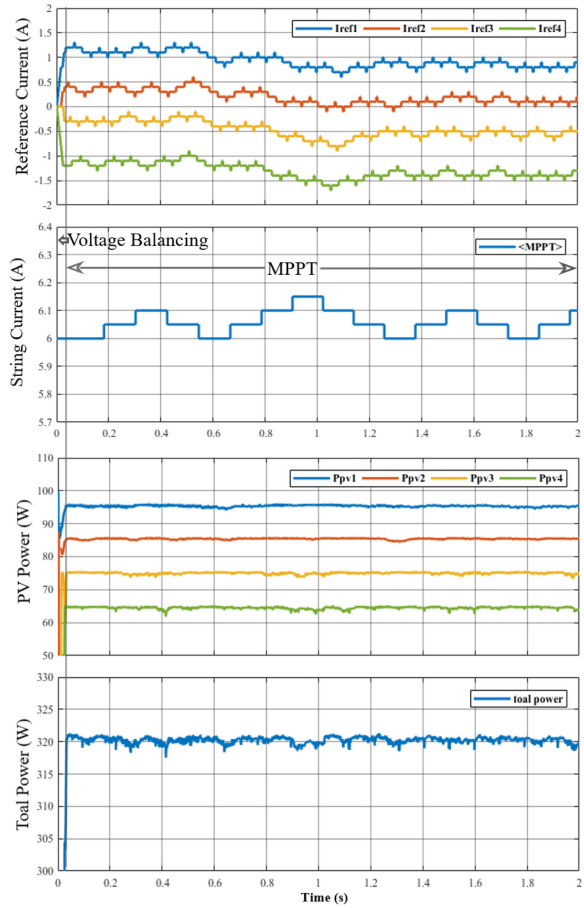

Fig. 12. Simulation results with one segmented DPP unit, showing waveforms for the four reference currents, string current, four PV powers, and total power.

A. *Simulation Results With One Unit*

Fig. 12 shows the results of the simulation with the irradiance conditions given in Fig. 11. Initially, all the reference currents are 0 A, indicating that the DPP converters are not operating. Since the four PV voltages are not the same, the controller operates

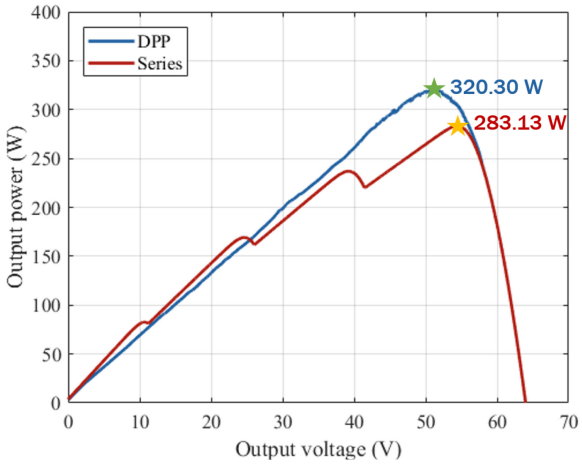

Fig. 13. Power-voltage curves for four PV panels.

in voltage balancing mode. As shown in Fig. 11, the reference values of DPP converters 1 and 4 step in opposite directions as do DPP converters 2 and 3 to a lesser degree until approximately 0.05 s, when the controller switches to MPPT mode. In MPPT, the short pulses in the reference current waveforms occur when the algorithm perturbs the system, but the new measured power is lower than the previous power; thus, the reference value returns immediately to the previous value. Since the current generated by PV1 and PV2 are higher than that of PV3 and PV4, the reference currents of DPP converters 1 and 2 are positive while those for DPP converters 3 and 4 are negative, as shown in the top graph of Fig. 12. The inverter P&O algorithm runs at a slower rate, as shown in the bottom graph of Fig. 12, while the segmented DPP MPPT algorithm runs about four times faster to optimize the unit's operation at each string current value. Over 1.2 s of the simulation, the overall system reaches an average power of 320 W (ideal maximum PV power is 321 W) and maintains operation at the MPP. This simulation verifies that the proposed control algorithm for the segmented DPP unit works properly to maximize produced power.

A sweep simulation was also conducted to compare the output power curve of the segmented DPP system with a series-connected PV system. The results are shown in Fig. 13, where the DPP system MPP is 13% higher than that of the series system. Further, the series-connected PV system exhibits multiple power peaks while the segmented DPP system has one global maxima, which is better for inverter interaction [24].

B. Simulation Results With Two Units

The segmented DPP unit is specially designed for modularity, where multiple segmented DPP units are used in one system. To confirm proper operation with multiple units, two segmented DPP units were simulated with eight PV panels. The shading conditions, irradiance level, and resulting power for each panel are shown in Fig. 14, based on a building self-shading scenario of the target BIPV system. Unit 1 is connected to the first row of four PV panels, where the power of PV 1–4 are 43.30, 54.10, 95.70, and 95.70 W, respectively, with a sum of 288.80 W.

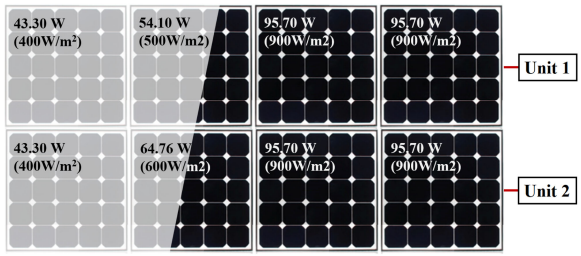

Fig. 14. Simulated shading conditions for eight PV panels.

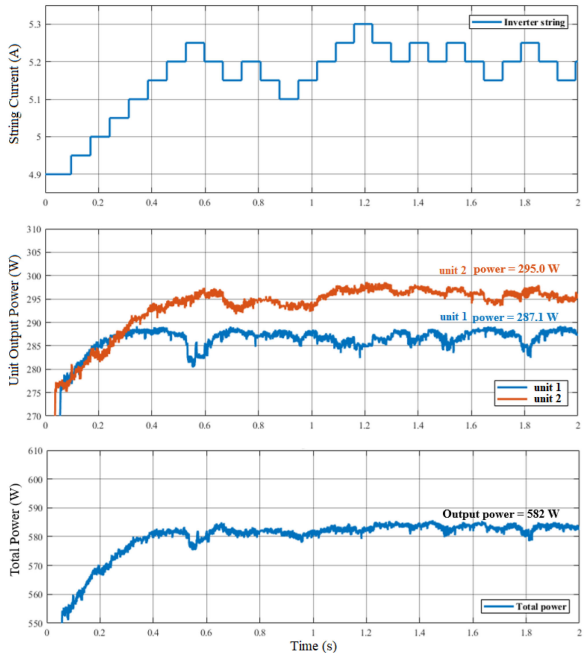

Fig. 15. Simulation results for the two-unit DPP system, showing waveforms for the string current, output power of both units, and total power.

Unit 2 is connected to the second row of panels, where the power of PV panels are the same, except the second panel's power is 67.76 W, and the sum is 299.46 W. The two segmented DPP units in series are connected to the inverter block running P&O MPPT in simulation.

As shown in Fig. 15, the inverter string current moves the system toward the overall MPP and stabilizes the string current. After 1.6 s, the three-step up and down pattern of the string current indicates that the P&O algorithm has stabilized around the MPP. The controller of each segmented DPP unit optimizes its output power; however, there is some variation in the power of each unit, which is a result of the unit's internal control continually perturbing the system to maintain operation near the unit's MPP. Once the system has stabilized, the variation in power of each unit is up to 8 W, but the variation in power of the total power is lower than 5 W. Unit 1 stabilizes at 287.1 W and Unit 2 stabilizes at 295.0 W, which is 582.1 W in total. These results verify that the segmented DPP units with independent control are able to interact with the inverter MPPT algorithm to optimize power produced for each unit. Further, the

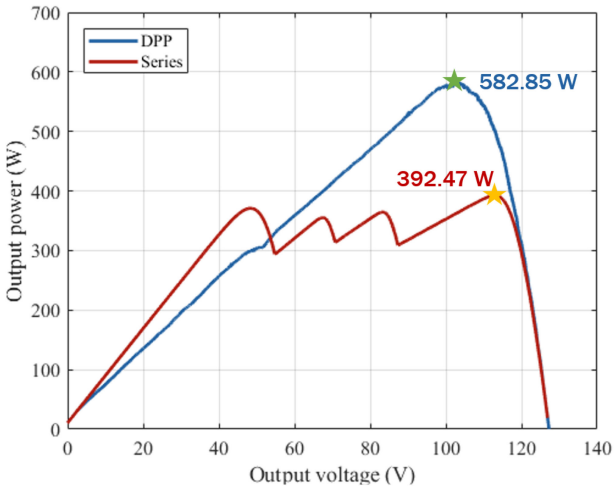

Fig. 16. P-V curve for the simulated two-unit DPP system.

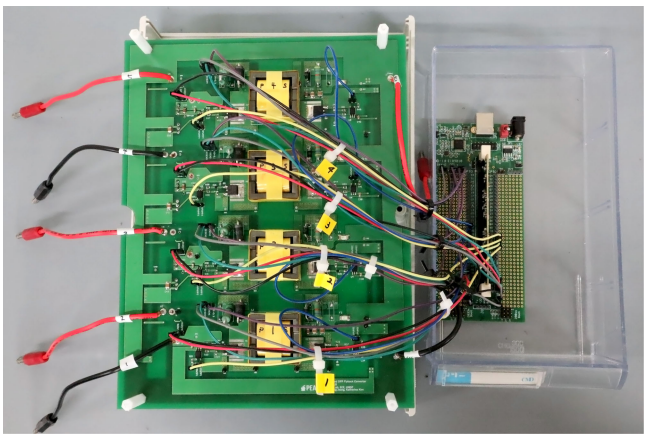

Fig. 17. Segmented DPP unit hardware.

independently controlled DPP units can be connected in series and scaled up to higher voltage systems.

Also, Fig. 16 compares the voltage sweep results of the segmented DPP and series-connected PV systems for the irradiance condition given in Fig. 14. The maximum power achieved by the segmented DPP system is 48.5% higher than that of the series-connected PV system. Again, the series-connected system exhibits distinct peaks, which means that the inverter may operate the series-connected system at a nonglobal maximum. Effectively, the PV panels connected to one segmented DPP unit act as an equivalent large panel.

VI. Segmented DPP System Experimental Results

A hardware prototype of the segmented DPP unit was also developed to verify its operation. The prototype consisted of four bidirectional flyback converters and a TMS320F28335 DSP to implement the control algorithm. The four flyback converters are implemented on one board and connected to a TMS320F28335 DSP controller board, as shown in Fig. 17. Each PV panel consists of 25 series-connected monocrystalline Si cells, with

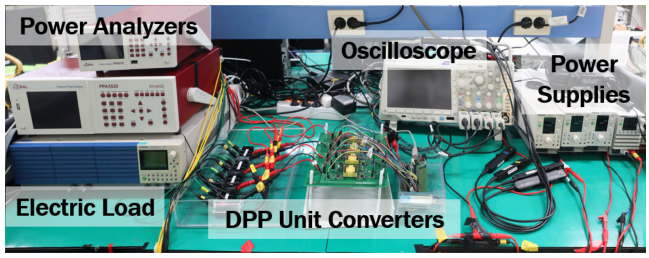

Fig. 18. Experimental setup with equipment.

the panel's MPP at 8.3 A and 12.8 V (105 W), under standard test conditions of 1000 W/m^2 and 25° C. A power analyzer was used to measure the voltage and current of the PV panels. A dc electronic load was used to emulate inverter operation and measure the load power. This equipment was connected to a computer running Python scripts that controlled the electronic load and acquired the measured data. Fig. 18 shows the diagram of the experimental setup and equipment. The experiments were conducted with this equipment setup, and the series string and the segmented DPP systems are compared under various emulated light conditions.

To create realistic and consistent PV panel characteristics during an experiment, a laboratory PV emulation method was used that was introduced and verified in [26]. This PV emulation method uses a power supply and a PV panel connected in parallel to emulate the realistic characteristics of the PV panel. The power supply in constant-current mode acts as an external controllable PV photocurrent and the PV panel surface is covered to ensure that actual photocurrent is not generated. Using this PV emulation method, experiments were conducted with four PV panels and four power supplies.

A. Bidirectional Flyback DPP Converter Efficiency

First, the bidirectional flyback converter was tested to determine the conversion efficiency of an individual DPP converter. The conversion efficiency was measured in both the forward and reverse directions. Fig. 19 shows the efficiency of the flyback converter according to the input power and the dashed line represents the efficiency including the power loss of the linear regulators and sensors. As shown, the power stage conversion efficiency is greater than 80% over the range of 5–25 W in both directions, with the maximum forward efficiency at 90.42% and maximum reverse efficiency at 87.52% (excluding sensor loss). This converter efficiency is similar to that of other bidirectional flyback converters used in DPP applications, such as [27] at 90% in the forward direction and 88% in the reverse direction at 25 W, and [28] that reached around 91% in the forward direction at 25 W. The advantage of DPP systems is that the power efficiency of the system is not limited by the converter efficiency and can be substantially higher than the converter efficiency [9].

B. Evaluation Metrics

In order to evaluate the PV system performance, the following metrics are utilized. MPP tracking efficiency measures how

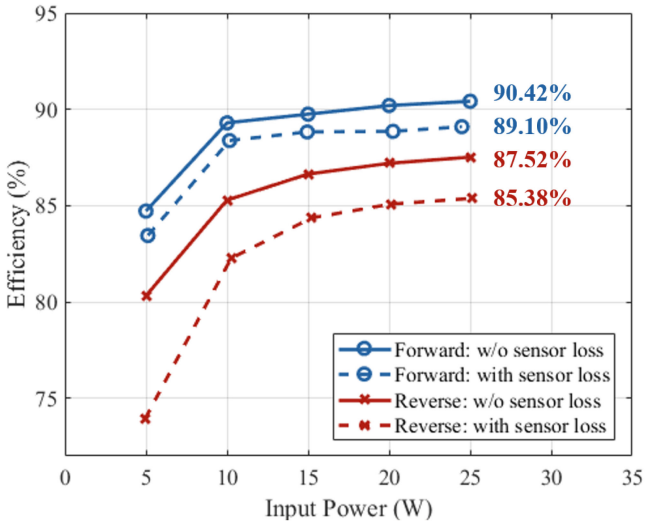

Fig. 19. Efficiency of the bidirectional flyback converter.

effectively the control algorithm maximizes PV power relative to the true MPP, which is defined as

$$\eta_{\text{MPPT}} = \frac{\sum_{k=1}^{n} P_{\text{PV},k}}{\sum_{k=1}^{n} P_{\text{MPP},k}} \tag{5}$$

where $P_{\text{PV},k}$ is the actual power produced by PV k and $P_{\text{MPP},k}$ is the true MPP of PV k. In other words, the sum of $P_{\text{PV},k}$ is the generated PV power from k panels and the sum of $P_{\text{MPP},k}$ is the ideal maximum power of the PV system. Next, segmented DPP unit efficiency is defined as

$$\eta_{\text{unit}} = \frac{P_{\text{out}}}{\sum_{k=1}^{n} P_{\text{PV},k}} \tag{6}$$

where P_{out} is the power output of the segmented DPP module, which includes converter, auxiliary circuit, and controller losses. Finally, system efficiency considers the output power relative to the ideal maximum of the PV system, which is defined as

$$\eta_{\text{sys}} = \frac{P_{\text{out}}}{\sum_{k=1}^{n} P_{\text{MPP},k}} = \eta_{\text{MPPT}} \times \eta_{\text{unit}}. \tag{7}$$

System efficiency is the main metric used to evaluate the overall performance for the segmented DPP system.

C. Startup

The segmented DPP unit was tested in experiment with four PV panels to observe the startup transient and settling time of the algorithm. Fig. 20 shows the input current waveforms (I_{DPP1} to I_{DPP4}) for the four DPP flyback converters after startup. Here, the PV panels are under even lighting conditions such that the variation is due to differences in manufacturing and wire resistances. After the segmented DPP unit is turned on, the voltage balancing mode is enabled and the DPP currents adjust within 5 s. Then, the algorithm changes to MPPT mode such that the currents undergo minor adjustments to continually track the MPP. After 15 s, the DPP converter input currents stabilize to their respective steady-state values, two above zero

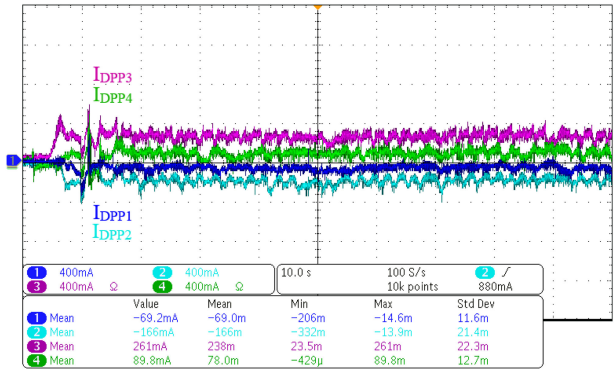

Fig. 20. DPP converter input currents after startup.

TABLE III
EXPERIMENTAL DATA AT DIFFERENT SHADING LEVELS

PV 4 Shade	P_{MPP} (W)	P_{in} (W)	P_{out} (W)	η_{unit}	η_{MPPT}	η_{sys}
Series-Connected System						
0%	328.09	328.07	318.41	97.06%	99.99%	97.05%
14.3%	317.30	301.39	292.80	97.15%	94.99%	92.28%
28.6%	306.20	256.48	249.73	97.37%	83.76%	81.56%
42.9%	294.94	242.67	234.16	96.49%	82.28%	79.39%
57.1%	283.12	243.76	234.49	96.20%	86.10%	82.82%
64.3%	274.32	241.68	231.37	95.73%	88.10%	84.34%
Segmented DPP System						
0%	326.99	326.79	315.14	96.43%	99.94%	96.38%
14.3%	317.65	316.28	302.33	95.59%	99.57%	95.18%
28.6%	307.01	306.52	293.42	95.73%	99.84%	95.57%
42.9%	294.57	293.97	277.44	94.38%	99.80%	94.18%
57.1%	282.19	281.69	263.04	93.63%	99.55%	93.21%
64.3%	274.04	273.13	254.04	93.01%	99.66%	92.70%

indicating forward operation and two below zero indicating reverse operation. The experimental waveforms are consistent with simulation waveforms, except that the time scale of the real system is longer because the algorithm's wait time was extended to 0.5 s to allow for the real segmented DPP system to sufficiently settle before new measurements were made. These results verify that startup operation works properly for a segmented DPP unit.

D. Effects of Increasing Partial Shading

Experiments were conducted to examine how well the segmented DPP unit can compensate for different shading levels. Six irradiance cases were tested where the emulated current of PVs 1–3 were maintained at 7 A and the current of PV 4 was varied. The current of PV 4 was tested at 7, 6, 5, 4, 3, and 2.5 A, which is equivalent to shading levels of 0%, 14.3%, 28.6%, 42.9%, 57.1%, and 64.3%, respectively. For each shading case, a sweep experiment was conducted using the segmented DPP prototype and compared to PV panels connected in series. The measurements and performance metrics for the six shading cases are summarized in Table III. The term P_{MPP} is the sum of true PV panel MPP, P_{in} is the measured input power from the PV panels, and P_{out} is the power measured at the load. For the series-connected PV system, η_{unit} indicates the efficiency of the cables connecting the PV panels to the electronic load.

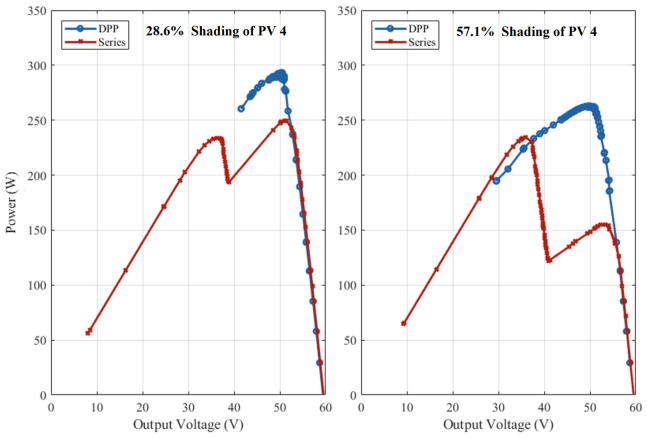

Fig. 21. P-V curves according to shading changes.

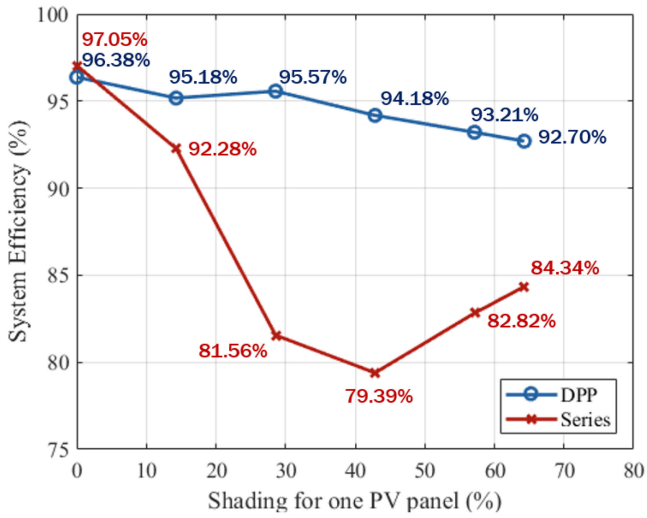

Fig. 22. System efficiency versus shading of one PV panel.

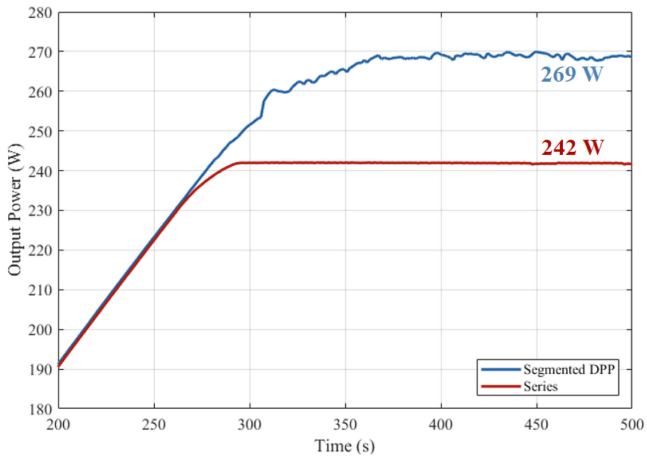

Fig. 23. Experimental results with inverter MPPT interaction.

Fig. 21 shows the power curves for two of the shading cases: 28.6% and 57.1% shading of PV 4. The series-connected PV panels show two power peaks and the power of the higher voltage peak decreases as the shading level increases. For the same shading cases, the segmented DPP system shows a single global maximum at a higher output power. This trait is consistent even when some of the DPP converters begin to reach their 2-A primary current limit, which is shown for the 57.1% shading case in Fig. 21. Note that the slope of the power curve is different below and above 36 V, which is a result of the DPP converter reaching its current limit. The DPP converter maintains operation at its current limit to offset as much of the current mismatch as possible, but the tracking efficiency (η_{MPPT}) begins to decrease.

In the series-connected system, the multiple power peaks, shown in Fig. 21, cause the MPPT efficiency to decrease. Conversely, the segmented DPP system maintains tracking efficiency over 99.66%, which follows the real MPP of each PV panel. As the shading level increases, current flowing through the DPP converters increases, which results in higher power loss through the converter and decreased system efficiency. Despite this converter loss, the segmented DPP system has higher system efficiency compared to the series-connected system in uneven lighting conditions. The system efficiency results for the range of shading cases are shown in Fig. 22. Except for the case with no shading, the segmented DPP unit consistently outperforms the series-connected PV panels with a maximum system efficiency improvement of 14.8%. The segmented DPP unit exhibits over 92.7% system efficiency even with severe shading (up to 64.3%) of one panel. Also, note that the segmented DPP system efficiency in all shading cases is higher than the peak efficiency of the bidirectional flyback converter in either the forward direction (89.1%) or reverse direction (85.4%).

E. Operation With Inverter MPPT

The segmented DPP unit's control was also tested to ensure effective interaction with an inverter running MPPT. An electronic load was used to control the string current according to the inverter P&O algorithm. The emulated photocurrents of the four PV panels were set to 7, 7, 5, and 5 A during the experiment. The experimental results are shown in Fig. 23 for the series-connected PV and segmented DPP systems. The output power of the series-connected system reaches 242 W at steady state while the segmented DPP system reaches a higher power of 269 W at steady-state operation. Although the segmented DPP system exhibits a wider power variation over time, it produces an average of 11.2% more power than the series-connected PV system. These results verify that the segmented DPP unit control properly adjusts to a given string current and interacts well with inverter MPPT control to optimize output power.

VII. Conclusion

This article introduced the segmented DPP system architecture, which utilizes modular design to take advantage of high power output enabled by DPP while allowing for straightforward installation. The segmented DPP unit approach allows for lower voltage ratings of the converters, fewer connectors, and simple wire connections compared to the conventional PV-to-bus DPP

architecture. The design assumes that standard PV panel cables plug directly into the segmented DPP unit and one additional cable connects between adjacent units. For this article, four PV panels were connected to one segmented DPP unit, which contained four bidirectional flyback converters and one digital controller. To control the segmented DPP unit, a system control algorithm was proposed that utilized both voltage balancing and MPPT modes to maximize PV power production. The control algorithm utilizes voltage balancing to quickly bring the PV panel voltages to the same value and then employs a type of P&O MPPT for the segmented DPP unit that optimizes each of the PV panels.

The operation and control of the segmented DPP system was first validated using simulation in MATLAB Simulink. The control algorithm was verified to maximize the output power of the segmented DPP system for a single unit and when multiple units are connected in series. An experimental prototype with four bidirectional flyback converters and a DSP controller was also developed and tested using an indoor testing setup with a controllable PV emulation method. The bidirectional flyback converters provided up to 2 A of primary-side current in both forward and reverse operations. The segmented DPP module consistently created a convex power curve with one global maximum point and exhibited higher output power compared to series connection in all uneven lighting conditions.

With the segmented DPP unit, system efficiency (including converter, auxiliary circuit, and controller power loss) was 96.38% under even lighting. With up to 64% shading on one of four PV panels, the segmented DPP unit maintained a system efficiency above 92.70% and increased system efficiency up to 14.8% compared to series connection. Experimental results also verified that the segmented DPP unit is independently controlled and effectively maximizes output power when operating with an inverter P&O MPPT algorithm. Future topics to improve upon this article are increasing the flyback converter efficiency to push the overall system efficiency higher and implementing a field study with multiple segmented DPP units to further evaluate performance. The segmented DPP unit takes advantage of DPP to maximize output power while allowing for modularity and ease of installation, which has higher potential for industry acceptance.

REFERENCES

[1] C. Olalla, C. Deline, D. Clement, Y. Levron, M. Rodriguez, and D. Maksimovic, "Performance of power-limited differential power processing architectures in mismatched PV systems," *IEEE Trans. Power Electron.*, vol. 30, no. 2, pp. 618–631, Feb. 2015.

[2] G. R. Walker and P. C. Sernia, "Cascaded DC-DC converter connection of photovoltaic modules," *IEEE Trans. Power Electron.*, vol. 19, no. 4, pp. 1130–1139, Jul. 2004.

[3] R. Pilawa-Podgurski and D. Perreault, "Submodule integrated distributed maximum power point tracking for solar photovoltaic applications," *IEEE Trans. Power Electron.*, vol. 28, no. 6, pp. 2957–2967, Jun. 2013.

[4] H. Jeong, H. Lee, Y. Liu, and K. A. Kim, "Review of differential power processing converters techniques for photovoltaic applications," *IEEE Trans. Energy Convers.*, vol. 34, no. 1, pp. 351–360, Mar. 2019.

[5] T. Shimizu, M. Hirakata, T. Kamezawa, and H. Watanabe, "Generation control circuit for photovoltaic modules," *IEEE Trans. Power Electron.*, vol. 16, no. 3, pp. 293–300, May 2001.

[6] Y. T. Jeon, H. Lee, K. A. Kim, and J. H. Park, "Least power point tracking method for photovoltaic differential power processing systems," *IEEE Trans. Power Electron.*, vol. 32, no. 3, pp. 1941–1951, Mar. 2017.

[7] B. Liu, S. Duan, and T. Cai, "Photovoltaic dc-building-module-based BIPV system—concept and design considerations," *IEEE Trans. Power Electron.*, vol. 26, no. 5, pp. 1418–1429, May 2011.

[8] POSCO, "POSCO Smart data center with the 'QR code' shaped BIPV," 2018. [Online]. Available: https://newsroom.posco.com/kr

[9] P. S. Shenoy, K. A. Kim, B. B. Johnson, and P. T. Krein, "Differential power processing for increased energy production and reliability of photovoltaic systems," *IEEE Trans. Power Electron.*, vol. 28, no. 6, pp. 2968–2979, Jun. 2013.

[10] J. Biswas, A. K. M, A. K. G., and M. Barai, "Design, architecture and real time distributed coordination DMPPT algorithm for PV systems," *IEEE J. Emerg. Sel. Top. Power Electron.*, vol. 6, no. 3, pp. 1418–1433, Sep. 2018.

[11] M. Uno and A. Kukita, "Two-switch voltage equalizer using an llc resonant inverter and voltage multiplier for partially shaded series-connected photovoltaic modules," *IEEE Trans. Ind. Appl.*, vol. 51, no. 2, pp. 1587–1601, Mar. 2015.

[12] M. Uno and A. Kukita, "Current sensorless equalization strategy for a single-switch voltage equalizer using multistacked buck-boost converters for photovoltaic modules under partial shading," *IEEE Trans. Ind. Appl.*, vol. 53, no. 1, pp. 420–429, Jan. 2017.

[13] K. A. Kim, P. S. Shenoy, and P. T. Krein, "Converter rating analysis for photovoltaic differential power processing systems," *IEEE Trans. Power Electron.*, vol. 30, no. 4, pp. 1987–1997, Apr. 2015.

[14] C. Olalla, D. Clement, M. Rodriguez, and D. Maksimovic, "Architectures and control of submodule integrated DC-DC converters for photovoltaic applications," *IEEE Trans. Power Electron.*, vol. 28, no. 6, pp. 2980–2997, Jun. 2013.

[15] E. E. Perl, J. Simon, J. F. Geisz, M. L. Lee, D. J. Friedman, and M. A. Steiner, "Measurements and modeling of III-V solar cells at high temperatures up to 400 °C," *IEEE J. Photovolt.*, vol. 6, no. 5, pp. 1345–1352, Sep. 2016.

[16] K. A. Kim, C. Xu, J. Lei, and P. T. Krein, "Dynamic photovoltaic model incorporating capacitive and reverse-bias characteristics," *IEEE J. Photovolt.*, vol. 3, no. 14, pp. 1334–1341, Oct. 2013.

[17] H. Jeong, H.-T. Cho, T. Kim, Y.-C. Liu, and K. A. Kim, "A scalable unit differential power processing system design for photovoltaic applications," in *Proc. IEEE Workshop Control Model. Power Electron.*, Jun. 2018, pp. 1–8.

[18] R. Bell and R. C. N. Pilawa-Podgurski, "Decoupled and distributed maximum power point tracking of series-connected photovoltaic submodules using differential power processing," *IEEE J. Emerg. Sel. Top. Power Electron.*, vol. 3, no. 4, pp. 881–891, Dec. 2015.

[19] G.-B. Koo, "Design guidelines for RCD snubber of flyback converters," Fairchild Semiconductor, Sunnyvale, CA, USA, Tech. Rep. AN-4147, 2006.

[20] S. Park *et al.*, "Design methodology of bidirectional flyback converter for differential power processing modules in PV applications," in *Proc. IEEE Int. Conf. Power Electron.-ECCE Asia*, May. 2019, pp. 1759–1764.

[21] D. W. Hart, *Power Electron.*. McGraw-Hill Companies, Inc., 1221 Avenue of the Americas, New York, NY, USA: McGraw-Hill Companies, Inc., 10020, 2011.

[22] M. G. Villalva, J. R. Gazoli, and E. R. Filho, "Comprehensive approach to modeling and simulation of photovoltaic arrays," *IEEE Trans. Power Electron.*, vol. 24, no. 5, pp. 1198–1208, May. 2009.

[23] G. Chu, H. Wen, L. Jiang, Y. Hu, and X. Li, "Bidirectional flyback based isolated-port submodule differential power processing optimizer for photovoltaic applications," *Sol. Energy*, vol. 158, pp. 929–940, 2017.

[24] T. Esram and P. L. Chapman, "Comparison of photovoltaic array maximum power point tracking techniques," *IEEE Trans. Energy Convers.*, vol. 22, no. 2, pp. 439–449, Jun. 2007.

[25] A. K. Abdelsalam, A. M. Massoud, S. Ahmed, and P. N. Enjeti, "High-performance adaptive perturb and observe MPPT technique for photovoltaic-based microgrids," *IEEE Trans. Power Electron.*, vol. 26, no. 4, pp. 1010–1021, Apr. 2011.

[26] S. Qin, K. A. Kim, and R. C. N. Pilawa-Podgurski, "Laboratory emulation of a photovoltaic module for controllable insolation and realistic dynamic performance," in *Proc. IEEE Power Energy Conf. Illinois*, Feb. 2013, pp. 23–29.

[27] C. Olalla, D. Clement, M. Rodriguez, and D. Maksimovic, "Architectures and control of submodule integrated dc-dc converters for photovoltaic applications," *IEEE Trans. Power Electron.*, vol. 28, no. 6, pp. 2980–2997, Jun. 2013.

[28] G. Chu, H. Wen, L. Jiang, Y. Hu, and X. Li, "Bidirectional flyback based isolated-port submodule differential power processing optimizer for photovoltaic applications," *Sol. Energy*, vol. 158, pp. 929–940, 2017.

Hoejeong Jeong (Student Member, IEEE) received the B.S. and M.S. degrees in electrical engineering from Ulsan National Institute of Science and Technology (UNIST), Ulsan, Korea, in 2017 and 2019, respectively.

She is a Researcher with LG electronics, Seoul, South Korea. Her research interests include PV systems and inverters for home appliances.

Ms. Jeong was the recipient of the Outstanding Undergraduate Student Award from the Korean Institute of Electrical Engineers (KIEE) in 2017.

Seungbin Park was born in Seoul, South Korea, in 1995. He received the B.S. degree in electrical engineering from Konkuk University, Seoul, South Korea, in 2018, and the M.S. degree in electrical and computer engineering from the Ulsan National Institute of Science and Technology (UNIST), Ulsan, South Korea, in 2020.

Since 2020, he has been with Dawonsys Co., Ltd., Ansan, Korea. His current research interests include isolated bidirectional dc-dc converters and power converters for PV applications.

Jee-Hoon Jung (Senior Member, IEEE) was born in Suwon, South Korea, in 1977. He received the B.S. degree in electrical engineering and the M.S. and Ph.D. degrees in electrical and computer engineering from the Department of Electronics and Electrical Engineering, Pohang University of Science and Technology (POSTECH), Pohang, South Korea, in 2000, 2002, and 2006, respectively.

From 2006 to 2009, he was a Senior Research Engineer with the Digital Printing Division, Samsung Electronics Company Ltd., Suwon, South Korea. From 2009 to 2010, he was a Postdoctoral Research Associate with the Department of Electrical and Computer Engineering, Texas A&M University at Qatar, Doha, Qatar. From 2011 to 2012, he was a Senior Researcher with the Power Conversion and Control Research Center, HVDC Research Division, Korea Electrotechnology Research Institute, Changwon, South Korea. From 2013 to 2016, he was an Assistant Professor with Electrical and Computer Engineering, Ulsan National Institute of Science and Technology (UNIST), Ulsan, South Korea, where he is presently working with Electrical Engineering as an Associate Professor. His current research interests include dc/dc and ac/dc converters, switched-mode power supplies, digital control and signal processing algorithms, power conversion for renewable energy, and real-time and power hardware-in-the-loop simulations of renewable energy and power grids. Recently, he has been researching high-frequency power converters using wide bandgap devices, bidirectional power converters for smart grids, power control algorithms, spread spectrum techniques and power line communications for dc microgrids, and high-frequency resonant inverters for induction heating applications.

Dr. Jung is a Senior Member of the IEEE Industrial Electronics Society, the IEEE Power Electronics Society, the IEEE Industry Applications Society (IAS), and the IEEE Power and Energy Society. He has served as an Asian Liason Officer for the Industrial Power Converter Committee in the IEEE IAS, a member of the Editorial Committee of the Korea Institute of Power Electronics (KIPE), and an Associate Editor for the *Journal of Power Electronics*. He is currently serving as a member of the Board of Directors of the KIPE. Also, he is an Editorial Board Member for Energies in the Multidisciplinary Digital Publishing Institute.

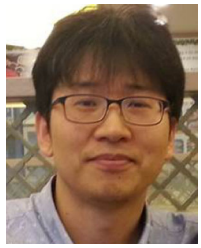

Taewon Kim received the B.S. degree in electronics engineering from Hanyang University, Seoul, South Korea, and the M.S. and Ph.D. degrees in electronic and electrical engineering from Pohang University of Science and Technology, Pohang, Korea, in 1997, 1999 and 2004, respectively.

From 2004 to 2008, he was with LG Electronics Digital Appliance Laboratory, Seoul, South Korea. He joined the Research institute of Industrial Science and Technology (RIST), Pohang, Korea, as a Senior Engineer. His current research interests include power conversion for renewable energy and capacitive deionization power converter.

A-Rong Kim received the B.S., M.S., and Ph.D. degrees in electrical engineering from the Changwon National University, Changwon, Korea, in 2006, 2008, and 2012, respectively.

Since 2011, she has been a Senior Researcher with the Research Institute of industrial Science and Technology (RIST), Pohang, Korea. Her research focuses on power system application of superconducting devices, analysis of power systems, and performance evaluation of BIPV. From February to July 2007, she was a Visiting Student with Chubu University, Nagoya, Japan. From March to September 2011, she was a Visiting Scholar with the Center for Advanced Power System (CAPS), Tallahassee, FL, USA.

Dr. Kim was the recipient of the Gold Color Engineering recognition at the Korean Society of Engineering Education in 2005, the Outstanding Presentation Award at Korea Institute of Applied Superconductivity and Cryogenics (KIASC) in 2009 and 2010, and the Best Student Award at Second Japan-Korea Superconductivity Workshop 2010 in Fukuoka, Japan.

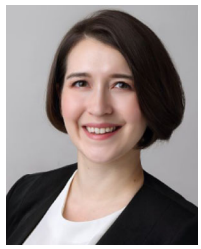

Katherine A. Kim (Senior Member, IEEE) received the B.S. degree in electrical and computer engineering from Franklin W. Olin College of Engineering, Needham, MA, USA, in 2007, and the M.S. and Ph.D. degrees in electrical and computer engineering from the University of Illinois, Urbana-Champaign, IL, USA, in 2011 and 2014, respectively.

From 2014 to 2018, she was an Assistant Professor of Electrical and Computer Engineering with the Ulsan National Institute of Science and Technology (UNIST), Ulsan, South Korea. Since 2019, she has been an Associate Professor of Electrical Engineering with National Taiwan University, Taipei, Taiwan. Her research focuses on power electronics and control for solar photovoltaic applications.

Dr. Kim was the recipient of the Graduate Research Fellowship in 2011 from the U.S. National Science Foundation. She was also the recipient of the Outstanding Teaching Award from UNIST in 2015, the Richard M. Bass Outstanding Young Power Electronics Engineer Award from the IEEE Power Electronics Society (PELS) in 2019, and was recognized as an Innovator Under 35 for the Asia Pacific Region by the MIT Technology Review in 2020. Since 2017, she has served as an Associate Editor for the IEEE TRANSACTIONS ON POWER ELECTRONICS. For IEEE PELS, she served as the Student Membership Chair from 2013 to 2014, PELS Member-At-Large from 2016 to 2018, and PELS Women in Engineering Chair from 2018 to 2020.